Synthesis and Single-Molecule Imaging of Highly Mobile Adamantane-Wheeled Nanocars

Pin-Lei E. Chu,[†] Lin-Yung Wang,[†] Saumyakanti Khatua, Anatoly B. Kolomeisky, Stephan Link,[*] and James M. Tour[*]

Department of Chemistry, Rice University, 6100 Main Street, Houston, Texas 77005, United States. [†]These authors contributed equally to this work.

ABSTRACT The synthesis and single-molecule imaging of two inherently fluorescent nanocars equipped with adamantane wheels is reported. The nanocars were imaged using 4,4-difluoro-4-bora-3a, 4a-diaza-s-indacene (BODIPY) as the chromophore, which was rigidly incorporated into the nanocar chassis *via* Sonogashira cross-coupling chemistry that permitted the synthesis of nanocars having different geometries. In particular, studied here were four- and three-wheeled nanocars with adamantane wheels. It was found that, for the four-wheeled nanocar, the percentage of moving nanocars and the diffusion constant show a significant improvement over *p*-carborane-wheeled nanocars with the same chassis. The three-wheeled nanocar showed only limited mobility due to its geometry. These results are consistent with a requisite wheel-like rolling motion. We furthermore developed a model that relates the percentage of moving nanocars in single-molecule experiments with the diffusion constant. The excellent agreement between the model and the new results presented here as well as previous single-molecule studies of fluorescent nanocars yields an improved understanding of motion in these molecular machines.

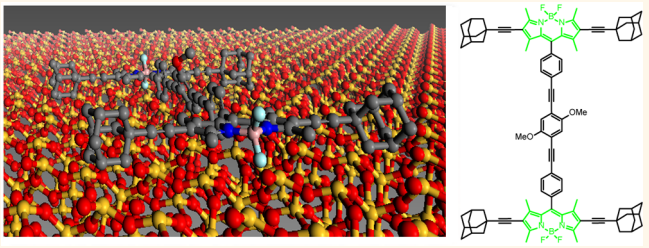

KEYWORDS: adamantane · nanocar · single-molecule fluorescence imaging · Sonogashira

Miniaturizing devices and machines such as motors,[1,2] switches,[3] turnstiles,[4] and barrows[5] to the molecular level has been accomplished by means of organic synthesis. These nanomachines were inspired by their macroscopic counterparts. A family of nanovehicles,[6] termed nanocars, was developed to translate on surfaces with controlled directionality. These nanocars are akin to their macroscopic analogues in the sense that they consist of a chassis, axles, and wheels. The ultimate goal would be to utilize nanocars to transport cargo from one place to another,[7] with the nanocars incorporating a device that imitates an engine, providing translational motion from an external energy source.[7−9]

The first generations of nanocars were equipped with carbon-based C_{60} wheels.[10,11] These nanocars demonstrated directional movement on a gold surface using a STM tip to electrically induce the motion. However, when trying to integrate a light-driven molecular motor that can convert light energy into rotational motion, it was found that the C_{60} wheels quenched the photoisomerization process of the molecular motor.[12−14] For this reason, *p*-carborane wheels were used, which are also spherical and can rotate symmetrically along a single bond. A series of *p*-carborane-wheeled nanocars with different functionalities have been synthesized, including a dipolar nanocar,[15] self-assembled nanocars,[16] nanotrains,[17] and a motorized nanocar.[7] Most of these nanocars were intended to be studied using scanning tunneling microscopy (STM) because this technique offers excellent atomic resolution. However, only few of them have been successfully imaged using STM, in large part due to the lengthy time periods often required to acquire high-quality STM images.

Seeking an alternative imaging method, single-molecule fluorescence microscopy (SMFM) was chosen to track individual nanocars and calculate their mobility on nonconductive substrates.[18,19] Even though this method does not provide the atomic resolution offered by STM, it allows localization of individual fluorophores within a few nanometers and also yields rapid results, two crucial requirements for progress in the field.

* Address correspondence to slink@rice.edu, tour@rice.edu.

Received for review October 3, 2012 and accepted November 27, 2012.

Published online November 27, 2012
10.1021/nn304584a

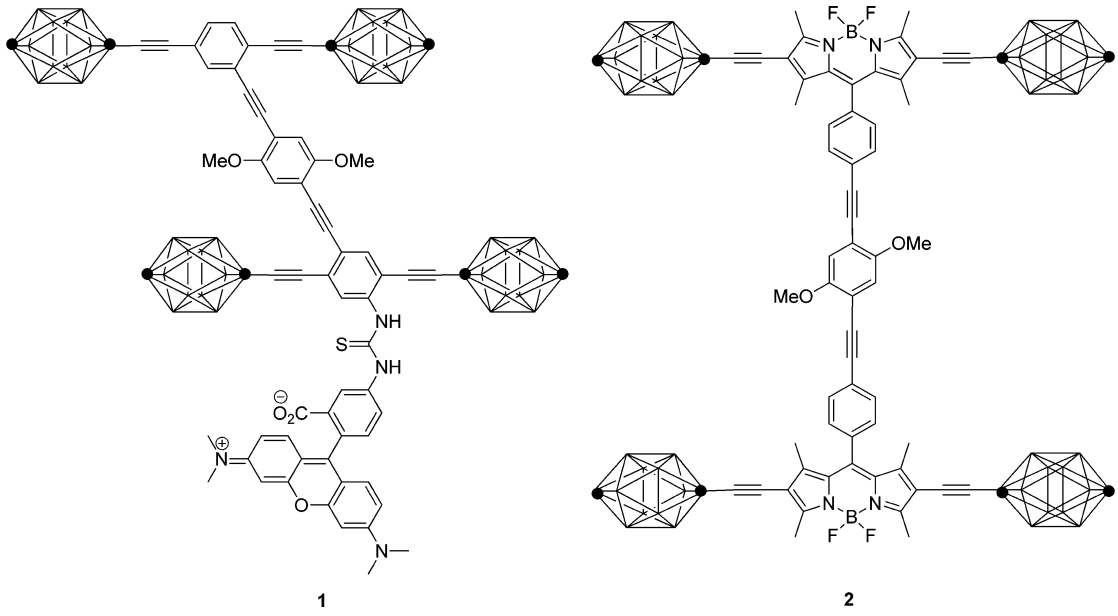

1 2

Figure 1. TRITC-tagged nanocar 1 and the four-wheeled *p*-carborane BODIPY nanocar 2.

The first approach to visualize nanocars on glass using SMFM involved attachment of the TRITC dye to the nanocars (**1** shown in Figure 1), but the nanocars showed low mobility (20−25% moving vehicles), possibly caused by strong electrostatic interactions between TRITC and the glass surface.[20,21] Next we synthesized a family of inherently fluorescent nanocars (**2** shown in Figure 1) featuring a 4,4-difluoro-4-bora-3a, 4a-diaza-s-indacene (BODIPY) core as part of the nanocar axles, which showed a significant increase in mobility (45% moving vehicles) compared to the TRITC-tagged nanocars.[18,22] However, nearly half of the BODIPY-based nanocars remained stationary under the imaging conditions. Since the ultimate goal is to use nanocars to transport nanocargo, it is desirable to maximize the number of moving molecules.

In order to maximize the number of moving nanocars, the surface−wheel interaction influences were studied. By recording the mobility of the BODIPY-based nanocar on different functionalized glass surfaces,[18] it was found that, when the hydrophilicity of the surface increases, the motion of nanocars is hindered *via* stronger interactions between the *p*-carborane wheels and the glass surface. Therefore, to modify the interactions between the glass surface and the nanocars, different wheels can be affixed. The geometry of the candidate should preferably be of comparable size to the nanocar, relatively spherical and symmetrical. Adamantane was chosen in the present work since it fulfills those requirements. Most importantly, it was hypothesized that the negligible polarity of its C−H bonds would lessen the interactions between the nanocar and the glass surface, thereby increasing the mobility of the nanocars. A size and shape comparison of three of our studied wheel systems, C_{60}, *p*-carborane, and adamantane, is shown on Figure 2.

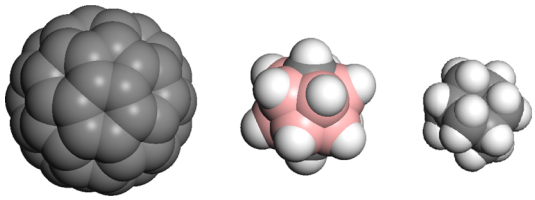

Figure 2. Space-filling models of C_{60}, *p*-carborane, and adamantane (from left to right).

Capitalizing upon the adamantane-wheeled systems, nanocar **3** in Scheme 1 was designed to move in a straight line on surfaces while the three-wheeled analogue **4** in Scheme 2 is expected to exhibit little or no motion given that only two of its three adamantane wheels are aligned.

To synthesize **3**, TMS-protected diiodide **5**[22] was coupled with ethynyladamantane (**6**)[23,24] to form **7**. After TMS deprotection, adamantane-wheel-axle **8** was obtained. Then two units of the terminal alkyne axle **8** were coupled with 1,4-diiodo-2,5-dimethoxybenzene (**9**)[25] to give **3**.

Trimer **4** was prepared through a Sonogashira coupling between triiodide BODIPY **10**[18] and terminal alkyne **6** (Scheme 2). It is noteworthy that the reaction was very efficient given that it was a triple coupling.

RESULTS AND DISCUSSION

The mobility of three different nanocars was investigated by single-molecule fluorescence imaging of the four- and three-wheeled adamantane nanocars **3** (Scheme 1) and **4** (Scheme 2); and the four-wheeled *p*-carborane nanocar **2**, shown in Figure 1. The latter

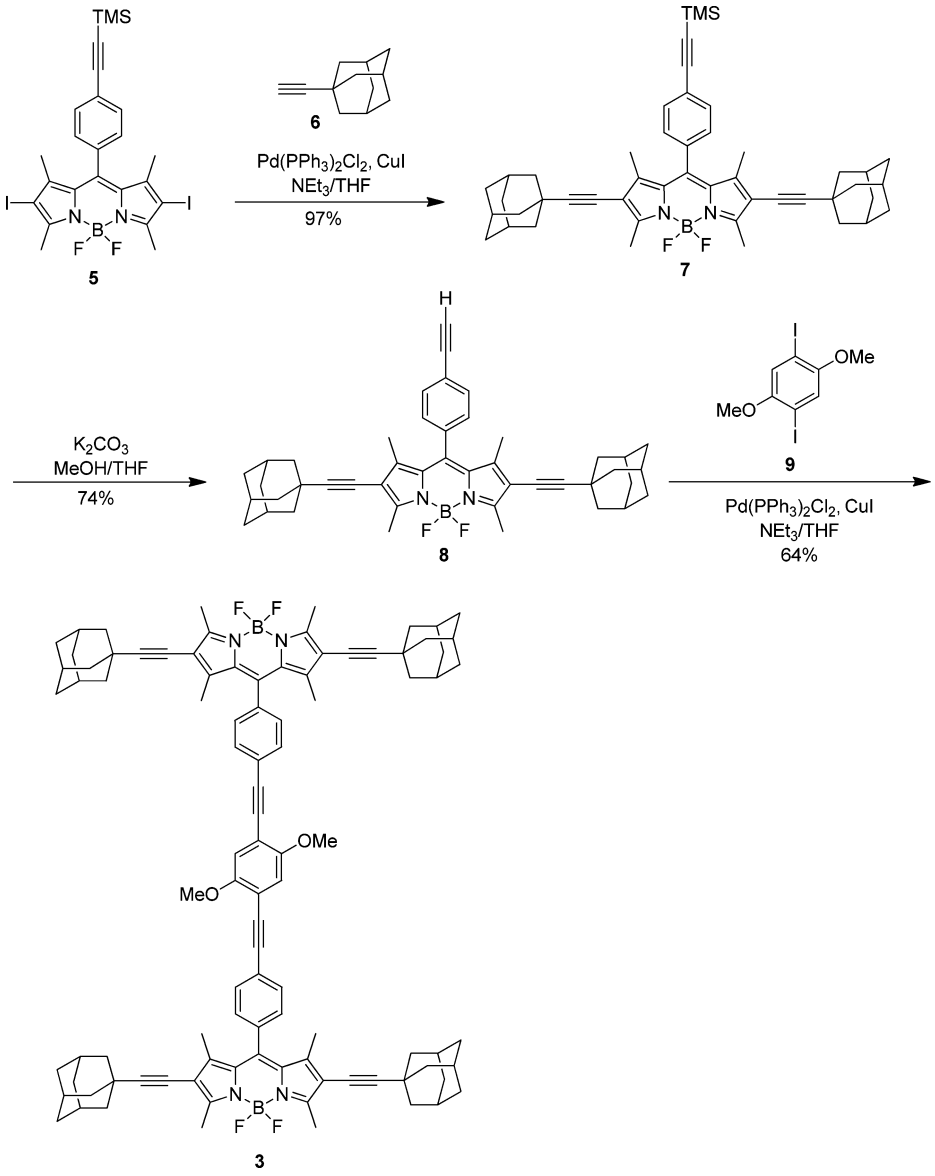

Scheme 1. Synthesis of adamantane-wheeled nanocar 3.

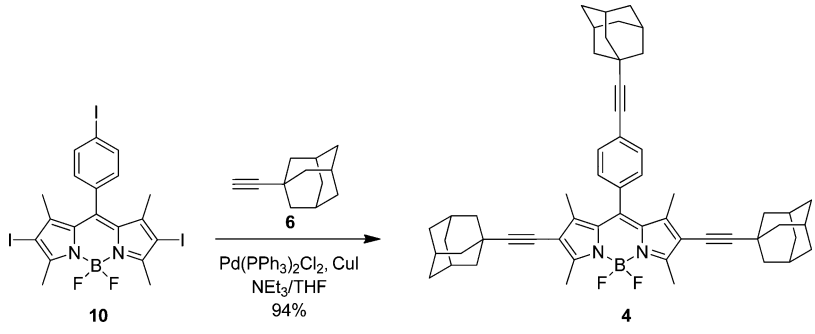

Scheme 2. Synthesis of adamantane-wheeled trimer 4.

has been studied previously and was measured here again for direct comparison between nanocars with the same chassis but different wheels.[18] An example of the fluorescence imaging is shown for **3** in Figure 3. The mobility of the nanocars was determined from fluorescence images taken as a function of time. Each series of time-lapse images contained 20 frames and was analyzed using a Matlab particle-tracking program, which can account for photoblinking and photobleaching of fluorescent molecules.[21] Specifically,

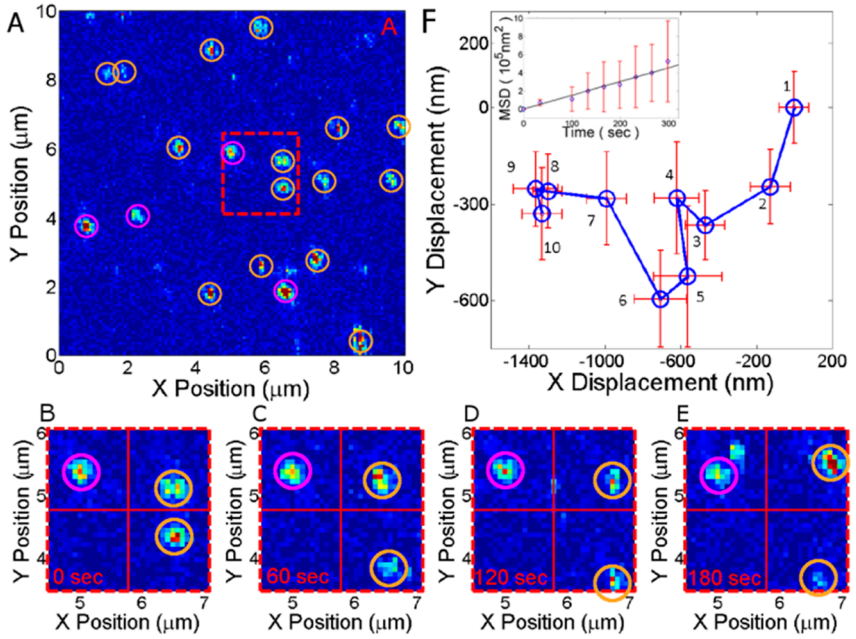

Figure 3. (A) Fluorescence image of 3. The yellow circles indicate moving nanocars, whereas the stationary nanocars are highlighted by purple circles. (B–E) Time-lapse images (2 μm × 2 μm) of the nanocars in the red dotted square in (A). The red cross at the center provides a reference frame to visualize the displacement of the two nanocars in the upper and lower right quadrants. (F) Single-molecule trajectory of 3. The error bars represent the *x*–*y* localization uncertainties determined from fitting a two-dimensional Gaussian function to the fluorescence spot in each image. The inset shows the mean square displacement as calculated from the trajectory as a function of time. The linear fit yields the diffusion constant.

the bright spots in the fluorescence image in Figure 3A represent individual nanocar molecules, which were identified based on an intensity threshold and the shape of the fluorescent spot. A two-dimensional Gaussian function was fit to each spot in the first image frame taken. The centroids of the Gaussian functions were regarded as the starting positions of the nanocars. Nanocars identified in subsequent frames were associated with those in previous frames, creating trajectories of position *versus* time for each individual molecule. To visually illustrate this, Figure 3B–E shows a time series of frames at a higher magnification for the red square marked in Figure 3A. The movement of individual nanocars is clearly seen in these images: the two nanocars in the upper and lower right quadrants move toward the outermost corners of their respective quadrants, while the bright spot in the upper left quadrant remains stationary and serves as a reference point. In Figure 3F, a single-molecule trajectory is provided as calculated from 10 fluorescence images until photobleaching occurred.

Molecules were categorized into "moving" and "stationary" nanocars based on the displacement compared to the localization error obtained from the Gaussian fit. If the displacement in at least two frames was larger than twice the localization error, the nanocars were considered to be moving. The ratio of moving nanocars marked by the yellow circles and stationary nanocars indicated by the purple circles is 15:4 for **3** (Figure 3). It should be noted that the threshold for identifying the moving nanocars was increased by a factor of 2 compared to earlier studies as we found that this threshold change allowed for a better distinction between moving and stationary nanocars, but otherwise, this threshold change had no significant effect on the results.

Two-dimensional diffusion constants for individual nanocars were calculated from single-molecule trajectories using a mean square displacement (MSD) analysis.[26,27] We have previously used an analysis that did not average the displacements for a given time interval, but instead gave each time step an equal weight.[18,21,20] Because recent simulations demonstrated that the MSD analysis generally yields a smaller uncertainty in the calculated diffusion constants,[26] we adopted this analysis for the current study. The MSD analysis for the single-molecule trajectory in Figure 3F is shown in the inset. By applying this procedure to all moving nanocars, their diffusion constants were calculated. The distributions of diffusion constants for all three nanocars studied here are summarized in Figure 4A, which also lists the average diffusion constants and percentages of moving nanocars. Errors for the average diffusion constant and the percentage of moving nanocars were calculated based on three independent measurements of at least 100 molecules each. Importantly, we tested the effects of all changes in the analysis procedure on the previously studied *p*-carborane-wheeled nanocar and found that the average diffusion constants and percentage of moving nanocars were comparable within the error of the measurement.

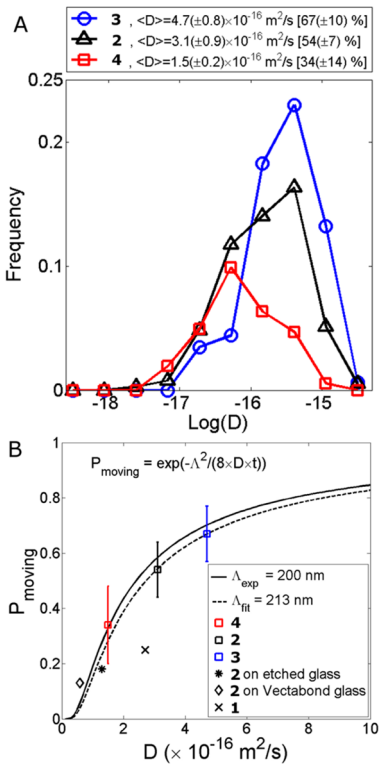

Figure 4. (A) Distribution of diffusion constants of the four-wheeled adamantane nanocar 3, three-wheeled adamantane trimer 4, and the BODIPY-based four-wheeled *p*-carborane nanocar 2. The average diffusion constants of the nanocars are shown in the legend. Percentages in the legend correspond to the fraction of moving nanocars and are proportional to the areas under the curves. (B) Fraction of moving nanocars P_{moving} as a function of the experimentally determined diffusion constant *D*. The data points also include previous measurements of the four-wheeled *p*-carborane nanocar 2 on different surfaces and a TRITC-tagged *p*-carborane nanocar 1.[18,20] The colored symbols in (B) correspond to the analogously colored lines shown in (A). The solid line was calculated from the two-dimensional random walk model (eq 2) with average experimental localization error of Λ_{exp} = 200 nm. The dashed line was calculated by fitting the data points to eq 2 instead, yielding a localization error of Λ_{fit} = 213 nm, which is in excellent agreement with experiments. Within experimental error, there is also excellent agreement between the measurements for 3 reported here and our earlier results, which were carried out independently from each other.

Comparing the two four-wheeled nanocars, which only differed by the type of wheel attached to the BODIPY-based chassis, we found that the new adamantane-wheeled nanocars **3** have a slightly larger diffusion constant (Figure 4A) compared to the *p*-carborane nanocars **2**. This result can be explained by the different interaction energies between the glass surface and the two different types of wheels. The adamantane wheels are hydrocarbons that interact with the glass *via* weak van der Waals forces. Such interactions are significantly smaller than the B−H···O hydrogen bonding between the *p*-carborane wheels with the oxygen of the glass substrate.[18−20] We focus on the interaction between nanocar wheels and substrate in this research. A discussion of the effect of surface roughness on the mobility of nanocars has been described in previous publications;[18] this prior research indicated that surface roughness affects the mobility of nanocars significantly less than the interaction of the wheels with the surface.

Assuming an energy-activated process for the nanocar movement, the fraction of moving nanocars is also an important characteristic of the nanocar mobility in experiments with finite measurement times, in addition to the diffusion constant, and should increase with increasing diffusion constant. This is indeed observed as illustrated by the integrated area under the histograms in Figure 4A, which also summarizes the values for the diffusion constant and fraction of moving nanocars. These results demonstrate our ability to tune the mobility of the nanocars through the interaction between the nanocar wheels and the substrate. While we previously changed the chemistry of the substrate,[18] here we have manipulated the nanocar movement by changing the wheels.

We can furthermore theoretically explain the relationship between the diffusion constant and the percentage of moving nanocars by a two-dimensional diffusion model that is based on the random walk theory. The probability $P(r,t)$ of finding a diffusing molecule on a two-dimensional surface can be expressed as eq 1:

$$P(r,t) = \frac{e^{-r^2/8Dt}}{\sqrt{8\pi Dt}} \quad (1)$$

where r is the radial distance from the starting position, t is the time, and D is the diffusion constant. Experimentally, the moving nanocars are those which move by more than twice the localization error Λ within the 30 s it takes to acquire an image. The fraction of moving nanocars P_{moving} can then be obtained by integrating $P(r,t)$ from $r = \Lambda$ to $r = \infty$, yielding eq 2:

$$P_{moving} = e^{-\Lambda^2/8Dt} \quad (2)$$

On the basis of this model, the fraction of moving nanocars is therefore directly related to the diffusion constant, in excellent agreement with our single-molecule imaging results. Using an average experimental localization error of Λ_{exp} = 200 nm, Figure 4B illustrates the relationship given by eq 2. The experimental data points for the three nanocars discussed here and summarized in Figure 4A are in excellent agreement with this model. Furthermore, we have included the data from our previous work on BODIPY-based *p*-carborane nanocars on different surfaces and a TRITC-tagged nanocar **1**, Figure 1.[18,20] Only the latter deviates from the predicted behavior, which is understandable considering that the TRITC dye was attached at the end of the nanocar chassis and likely impeded the movement of some nanocars by acting as a local surface anchor, thereby reducing the fraction of moving nanocars while not affecting the diffusion constant

for the mobile nanocars. In addition, a fit of the data points to eq 2 yields a localization error of Λ_{fit} = 213 nm, in excellent agreement with the experimentally estimated value for Λ.

Comparing the mobility of **3** *versus* **4** allowed us to again address the mechanism of the nanocar movement. **4** shows some mobility, but the diffusion constant and the percentage of moving nanocars decreased significantly compared to **3** (Figure 4). If the nanocars were only hopping or sliding on the surface, we would expect that the trimer **4** would show a higher mobility because they have one fewer wheel and thus reduced interaction energy with the substrate. However, we observed the opposite as **3** has a higher mobility than **4**. The small but nonzero mobility of **4** could be explained assuming that some of those nanocars move using only the two wheels aligned at 180° while the third wheel projects upward and occasionally acts as a brake when surface-bound. These results are therefore in excellent agreement with previous experimental studies and molecular dynamics simulations, which showed a wheel-assisted moving mechanism of nanocars.[11,20,28]

CONCLUSIONS

Our single-molecule measurements presented here not only support our previous study, which concluded that the interaction energy between the nanocar wheels and the glass substrate determines the mobility of the nanocars,[18,19] but also successfully demonstrate the feasibility of changing the wheels to further improve the mobility of nanocars, giving guidance for the future molecular design of efficient nanotransporters. The comparison of the diffusion constants and percentage of moving nanocars between the four-wheeled nanocar **3** and the three-wheeled nanocar **4** furthermore validates the wheel-like rolling mechanism suggested for the movement of these molecular machines.

EXPERIMENTAL SECTION

Materials and Methods. Glass coverslips (Fisher Scientific 12-545-F 24X50-1) were used as the substrate. They were first cleaned by sonication in soap (LIQUIDNOX, ALCONOX) for 15 min, rinsed with DI water, and then dried with nitrogen. The cleaning steps were repeated three times before oxygen plasma cleaning (Harrick Plasma PDC-32G) at ~200 mTorr for 2 min. The cleaned coverslips were stored in DI water until used. Single-molecule fluorescence imaging was carried out on a home-built sample scanning fluoresecnce microscope that is schematically illustrated in Figure S1 in the Supporting Information. Circularly polarized 514 nm excitation was provided by an Ar^+ laser (Modu-Lasser Stellar-Pro). The laser beam was expanded before entering an inverted microscope (Zeiss Axiovert 200) to achieve a diffraction-limited excitation spot. Fluorescence was collected in an epi-illumination geometry by an oil-immersion objective (Zeiss Fluar) and then directed to an avanlanche photodiode detector (Perkin-Elmer SPCM-AQR-15). The oil is used to match the refractive index to that of the coverslip, thereby increasing the collection angle for the emitted fluorescence, as it is important to collect as many photons as possible in these single-molecule experiments. The oil is in contact with the objective and the bottom surface of the coverslip; the nanocars are on top of the glass coverslip. Therefore, the oil does not contact the nanocars. A dichroic mirror and a notch filter were used to separate the fluorescence from the excitation beam. The samples were placed on a *XYZ* piezoelectric scanning stage (Physik Instrumente P-517.3CL), which was controlled by a surface probe controller (RHK Technology SPM 1000). Images with dimensions of 10 μm × 10 μm consisting of 128 × 128 pixels were acquired by moving the sample across the excitation spot with a scanning speed of 1 pixel/ms. Typical excitation powers at the sample were 500 nW. All measurements were carried out at room temperature and in an ambient air atmosphere.

Synthetic Procedure. *General Methods.* Reagent grade tetrahydrofuran (THF) was distilled from sodium benzophenoneketyl. Triethylamine (Et_3N) and dichloromethane (CH_2Cl_2) were distilled from CaH_2 under a N_2 atmosphere. THF and Et_3N were degassed with a stream of argon for 30 min before being used in the Sonogashira coupling reactions. All other chemicals were purchased from commercial suppliers and used without further purification. Flash column chromatography was performed using 230−400 mesh silica gel from EM Science.

Synthesis of 7. An oven-dried 10 mL Schlenk tube equipped with a stir bar was charged with TMS-protected diiodide **5**[22] (100 mg, 0.149 mmol), **6**[23,24] (53 mg, 0.33 mmol), $Pd(PPh_3)_2Cl_2$ (10.4 mg, 14.8 μmol), and CuI (5.7 mg, 30 μmol) to which were added Et_3N (2 mL) and THF (1 mL). The reaction mixture was stirred at 70 °C overnight. The mixture was quenched with saturated NH_4Cl (20 mL) and extracted with dichloromethane (60 mL). The organic phase was washed with water (30 mL), dried over anhydrous $MgSO_4$, filtered, and the filtrate was concentrated under vacuum. The crude product was purified by column chromatography (silica gel, 5% EtOAc in hexanes) to yield **7** as a red solid (106 mg, 97%): FTIR (neat) 2904, 2848, 2162, 1616, 1526, 1475, 1390, 1310, 1220, 1175, 1077 cm^{-1}; ^1H NMR (500 MHz, $CDCl_3$) δ 7.60 (d, J = 8.5 Hz, 2H), 7.19 (d, J = 8.5 Hz, 2H), 2.59 (s, 6H), 1.96 (M, 6H), 1.90 (d, J = 2.9 Hz, 12H), 1.69 (t, J = 3.0 Hz, 12H), 1.42 (s, 6H), 0.28 (s, 9H); ^{13}C NMR (125 MHz, $CDCl_3$) δ 158.46, 143.27, 141.04, 135.30, 133.08, 130.96, 128.38, 124.41, 117.22, 106.27, 104.49, 96.29, 71.27, 43.43, 36.68, 30.79, 28.34, 13.82, 13.78, 0.23; HRMS (APCI) m/z calcd for $[M + H]^+$ $C_{48}H_{55}N_2BF_2Si$ 737.4277, found 737.4306.

Synthesis of 8. An oven-dried 25 mL round-bottom flask equipped with a stir bar was charged with **7** (100 mg, 0.136 mmol) and K_2CO_3 (94 mg, 0.68 mmol) to which were added MeOH (5 mL) and THF (5 mL). The reaction mixture was stirred at room temperature for 90 min. The mixture was quenched with water and extracted with dichloromethane (50 mL). The organic phase was washed with water (30 mL), dried over anhydrous $MgSO_4$, filtered, and the filtrate was concentrated under vacuum. The crude product was purified by column chromatography (silica gel, 5% EtOAc in hexanes) to yield **8** as a dark red solid (67 mg, 74%): FTIR (neat) 3263, 2901, 2850, 1616, 1536, 1475, 1400, 1305, 1225, 1170, 1077 cm^{-1}; ^1H NMR (500 MHz, $CDCl_3$) δ 7.63 (d, J = 8.3 Hz, 2H), 7.22 (d, J = 8.5 Hz, 2H), 3.19 (s, 1H), 2.59 (s, 6H), 1.97 (s, 6H), 1.90 (d, J = 2.9 Hz, 12H), 1.70 (d, J = 3.0 Hz, 12H), 1.42 (s, 6H); ^{13}C NMR (125 MHz, $CDCl_3$) δ 158.52, 143.25, 140.83, 135.69, 133.22, 130.94, 128.52, 123.44, 117.28, 106.30, 83.18, 79.00, 71.26, 43.43, 36.68, 30.79, 28.34, 13.83, 13.76; HRMS (APCI) m/z calcd for $[M + H]^+$ $C_{45}H_{47}BF_2N_2$ 665.3879, found 665.3909.

Synthesis of 3. An oven-dried 10 mL Schlenk tube equipped with a stir bar was charged with **8** (50 mg, 0.075 mmol), **9**[24] (13.4 mg, 0.034 mmol), $Pd(PPh_3)_2Cl_2$ (5.3 mg, 7.6 μmol), and CuI (2.9 mg, 15 μmol) to which were added Et_3N (1 mL) and THF (1 mL). The reaction mixture was stirred at room temperature overnight. The mixture was quenched with saturated NH_4Cl (10 mL) and extracted with dichloromethane (30 mL).

The organic phase was washed with water (20 mL), dried over anhydrous $MgSO_4$, filtered, and the filtrate was concentrated under vacuum. The crude product was purified by column chromatography (silica gel, 30% chloroform in hexanes) to yield **3** as a purple solid (70.4 mg, 64%): FTIR (neat) 2900, 2850, 1616, 1530, 1480, 1450, 1392, 1310, 1225, 1172, 1075 cm^{-1}; ^1H NMR (400 MHz, CD_2Cl_2) δ 7.70 (d, J = 7.9 Hz, 4H), 7.29 (d, J = 7.8 Hz, 4H), 7.09 (s, 2H), 3.91 (s, 6H), 2.54 (s, 12H), 1.94 (M, 12H), 1.90 (M, 24H), 1.69 (M, 24H), 1.46 (s, 12H); ^{13}C NMR (125 MHz, $CDCl_3$) δ 158.51, 154.32, 143.22, 141.06, 135.25, 132.80, 131.00, 128.51, 124.48, 117.25, 115.89, 113.57, 106.29, 94.80, 87.35, 71.27, 56.84, 43.43, 36.68, 30.80, 28.34, 13.83, 13.80; MALDI m/z calcd for $[M + K]^+$ $C_{98}H_{100}B_2F_4N_4O_2$ 1502.8, found 1502.7.

Synthesis of 4. An oven-dried 10 mL Schlenk tube equipped with a stir bar was charged with triiodide BODIPY **10**[18] (200 mg, 0.285 mmol), **6**[23,24] (160 mg, 1.0 mmol), $Pd(PPh_3)_2Cl_2$ (30 mg, 0.043 mmol), and CuI (16.3 mg, 0.086 mmol) to which were added Et_3N (2 mL) and THF (2 mL). The reaction mixture was stirred at room temperature overnight. The mixture was quenched with saturated NH_4Cl (25 mL) and extracted with dichloromethane (100 mL). The organic phase was washed with water (50 mL), dried over anhydrous $MgSO_4$, filtered, and the filtrate was concentrated under vacuum. The crude product was purified by column chromatography (silica gel, 10% EtOAc in hexanes) to yield **4** as a red solid (214.3 mg, 94%): FTIR (neat) 2900, 2848, 1616, 1530, 1450, 1391, 1309, 1225, 1175, 1075 cm^{-1}; ^1H NMR (500 MHz, $CDCl_3$) δ 7.52 (d, J = 8.5 Hz, 2H), 7.15 (d, J = 8.5 Hz, 2H), 2.59 (s, 6H), 2.08 − 1.61 (m, 45H), 1.43 (s, 6H); ^{13}C NMR (125 MHz, $CDCl_3$) δ 158.29, 143.41, 141.51, 134.08, 132.75, 131.08, 128.20, 125.44, 117.11, 106.18, 100.21, 79.17, 71.33, 43.44, 43.08, 36.68, 30.78, 30.51, 28.31, 28.27, 13.82, 13.80; HRMS (APCI) m/z calcd for $[M + H]^+$ $C_{55}H_{61}BF_2N_2$ 799.4978, found 799.4966.

Conflict of Interest: The authors declare no competing financial interest.

Acknowledgment. Funding was provided by The National Science Foundation (CHE-1007483). S.L. also acknowledges support from the Robert A. Welch Foundation (C-1664).

Supporting Information Available: Figures and NMR spectra. This material is available free of charge *via* the Internet at http://pubs.acs.org.

REFERENCES AND NOTES

1. Klok, M.; Boyle, N.; Pryce, M. T.; Meetsma, A.; Browne, W. R.; Feringa, B. L. Unidirectional Rotation of Molecular Rotary Motors. *J. Am. Chem. Soc.* **2008**, *130*, 10484–10485.
2. Kulago, A. A.; Mes, E. M.; Klok, M.; Meetsma, A.; Brouwer, A. M.; Feringa, B. L. Ultrafast Light-Driven Nanomotors Based on an Acridane Stator. *J. Org. Chem.* **2010**, *75*, 666–679.
3. Chiang, P.-T.; Cheng, P.-N.; Lin, C.-C.; Liu, Y.-H.; Lai, C.-C.; Peng, S.-H.; Chiu, S.-H. A Macrocycle/Molecular-Clip Complex That Functions as a Quadruply Controllable Molecular Switch. *Chem.—Eur. J.* **2006**, *12*, 865–876.
4. Bedard, T.; Moore, J. S. Design and Synthesis of Molecular Turnstiles. *J. Am. Chem. Soc.* **1995**, *117*, 10662–10671.
5. Rapenne, G.; Jimenez-Bueno, G. Molecular Machines: Synthesis and Characterization of Two Prototypes of Molecular Wheelbarrows. *Tetrahedron* **2007**, *63*, 7018–7026.
6. Shirai, Y.; Morin, J.-F.; Sasaki, T.; Guerrero, J. M.; Tour, J. M. Recent Progress on Nanovehicles. *Chem. Soc. Rev.* **2006**, *35*, 1043–1055.
7. Chiang, P.-T.; Mielke, J.; Godoy, J.; Guerrero, J. M.; Alemany, L. B.; Villagómez, C. J.; Saywell, A.; Grill, L.; Tour, J. M. Toward a Light-Driven Motorized Nanocar: Synthesis and Initial Imaging of Single Molecules. *ACS Nano* **2012**, *6*, 592–597.
8. Godoy, J.; Vives, G.; Tour, J. M. Toward Chemical Propulsion: Synthesis of ROMP-Propelled Nanocars. *ACS Nano* **2011**, *5*, 85–90.
9. Kudernac, T.; Ruangsupapichat, N.; Parschau, M.; Maciá, B.; Katsonis, N.; Harutyunyan, S. R.; Ernst, K.-H.; Feringa, B. L. Electrically Driven Directional Motion of a Four-Wheeled Molecule on a Metal Surface. *Nature* **2011**, *479*, 208–211.
10. Shirai, Y.; Osgood, A.; Zhao, Y.; Yao, Y.; Saudan, L.; Yang, H.; Yu-Hung, C.; Alemany, L. B.; Sasaki, T.; Morin, J.-F.; *et al.* Surface-Rolling Molecules. *J. Am. Chem. Soc.* **2006**, *128*, 4854–4864.
11. Shirai, Y.; Osgood, A. J.; Zhao, Y.; Kelly, K. F.; Tour, J. M. Directional Control in Thermally Driven Single-Molecule Nanocars. *Nano Lett.* **2005**, *5*, 2330–2334.
12. Shirai, Y.; Sasaki, T.; Guerrero, J. M.; Yu, B.; Hodge, P.; Tour, J. M. Synthesis and Photoisomerization of Fullerene−and Oligo(phenylene ethynylene)−Azobenzene Derivatives. *ACS Nano* **2008**, *2*, 97–106.
13. Sasaki, T.; Tour, J. M. Synthesis of a New Photoactive Nanovehicle: Nanoworm. *Org. Lett.* **2008**, *10*, 897–900.
14. Morin, J.-F.; Shirai, Y.; Tour, J. M. En Route to a Motorized Nanocar. *Org. Lett.* **2006**, *8*, 1713–1716.
15. Sasaki, T.; Tour, J. M. Synthesis of a Dipolar Nanocar. *Tetrahedron Lett.* **2007**, *48*, 5821–5824.
16. Sasaki, T.; Guerrero, J. M.; Tour, J. M. The Assembly Line: Self-Assembling Nanocars. *Tetrahedron* **2008**, *64*, 8522–8529.
17. Sasaki, T.; Guerrero, J. M.; Leonard, A. D.; Tour, J. M. Nanotrains and Self-Assembled Two-Dimensional Arrays Built from Carboranes Linked by Hydrogen Bonding of Dipyridones. *Nano Res.* **2008**, *1*, 412–419.
18. Khatua, S.; Godoy, J.; Tour, J. M.; Link, S. Influence of the Substrate on the Mobility of Individual Nanocars. *J. Phys. Chem. Lett.* **2010**, *1*, 3288–3291.
19. Kupchenko, I.; Moskovsky, A.; Nemukhin, A. V.; Kolomeisky, A. B. On the Mechanism of Carborane Diffusion on a Hydrated Silica Surface. *J. Phys. Chem. C* **2011**, *115*, 108–111.
20. Khatua, S.; Guerrero, J.; Claytor, K.; Vives, G.; Kolomeisky, A. B.; Tour, J. M.; Link, S. Monitoring of Individual Nanocars on Glass. *ACS Nano* **2009**, *3*, 351–356.
21. Claytor, K.; Khatua, S.; Guerrero, J. M.; Tcherniak, A.; Tour, J. M.; Link, S. Accurately Determining Single Molecule Trajectories of Molecular Motion on Surfaces. *J. Chem. Phys.* **2009**, *130*, 164710.
22. Godoy, J.; Vives, G.; Tour, J. M. Synthesis of Highly Fluorescent BODIPY-Based Nanocars. *Org. Lett.* **2010**, *12*, 1464–1467.
23. Archibald, T. G.; Malik, A. A.; Baum, K.; Unroe, M. R. Thermally Stable Acetylenic Adamantane Polymers. *Macromolecules* **1991**, *24*, 5261–5265.
24. Negishi, E.; Baba, S. Convenient Method for the *Tertiary* Alkyl-Alkynyl Coupling *via* Organoalanes. *J. Am. Chem. Soc.* **1975**, *97*, 7385–7387.
25. Waybright, S. M.; Singleton, C. P.; Wachter, K.; Murphy, C. J.; Bunz, U. H. F. Oligonucleotide-Directed Assembly of Materials: Defined Oligomers. *J. Am. Chem. Soc.* **2001**, *123*, 1828–1833.
26. Michalet, X. Mean Square Displacement Analysis of Single-Particle Trajectories with Localization Error: Brownian Motion in an Isotropic Medium. *Phys. Rev. E* **2010**, *82*, 041914-1-13.
27. Savin, T.; Doyle, P. S. Static and Dynamic Errors in Particle Tracking Microrheology. *Biophys. J.* **2005**, *88*, 623–638.
28. Akimov, A. V.; Nemukhin, A. V.; Moskovsky, A. A.; Kolomeisky, A. B.; Tour, J. M. Molecular Dynamics of Surface-Moving Thermally Driven Nanocars. *J. Chem. Theory Comput.* **2008**, *4*, 652–656.